This is a repository copy of *Structural characterisation of porous copper sheets fabricated by lost carbonate sintering applied to tape casting*.

Article:

Structural Characterisation of Porous Copper Sheets Fabricated by Lost Carbonate Sintering Applied to Tape Casting.

Mosalagae Mosalagae[1,3,a]•, Carlos M Brambila Renteria[1,b] Mohammed Elbadawi[2,c] Mohammed Shbeh[1,d] and Russell Goodall[1,d]

[1*]Department of Material Science and Engineering, University of Sheffield, Sir Robert Hadfield Building, Mappin Street, Sheffield, S1 3JD, UK.

[2]Department of Mechanical Engineering, University of Sheffield, Mappin Building, Mappin Street, Sheffield, S1 3JD, United Kingdom.

[3]Department of Mechanical, Energy and Industrial Engineering, Faculty of Engineering and Technology, Botswana International University of Science and Technology, Plot 10071, Boseja Ward, Palapye, Private Bag 16, Botswana

[*] Corresponding author. tel.: +26772279039; e-mail: [a]mmosalagae1@sheffield.ac.uk, [b]cmbrambilarenteria1@sheffield.ac.uk, [c]melbadawi1@sheffield.ac.uk, mmmshbeh1@sheffield.ac.uk [d]r.goodall@sheffield.ac.uk

Key words: Porous copper, Lost Carbonate Sintering, Tape casting, Heat sinks, Space holder, Porosity,

In this article, we describe experimental investigations of the structural characterisations of double-layered porous copper tapes of thickness down to 0.74 mm. The porous sheets were produced by a process combing tape casting and lost carbonate sintering (LCS) to control both the porosity and pores distribution of the sheets. By varying the values of processing parameters, double-layer (porous and dense) structured tapes with open cell structure and porosities ranging from 50.0 – 81.5% are produced. Scanning electron microscopy and actual size image analysis were employed to measure the pore size and surface porosity of the porous sample. The pore size distribution was characterised using Micro-CT scanner running Skyscan *NRecon* software and *CTAn* software. A helium pycnometer was employed to obtain the bulk porosity of the porous copper samples. Statistical analysis of these measurements was used to assess the efficiency and consistency of the space holder technique used to generate porosity, as well as to draw information about the influence that different processing routes have on the resulting mesostructure of the porous copper metal, and on its properties.

1. Introduction

Recently, heat dissipation requirements for small portable electronic devices operating at high frequency have been increasing, as these components gets smaller and power usage increases. However, convectional passive cooling techniques are often inadequate for high rates of heat

dissipation and hence, active cooling techniques are likely to be more suitable for this purpose. Heat exchangers with small size yet relatively high heat transfer performance are required to cool these devices to ensure system speed, system durability and reliability are maintained. Open cell porous copper maybe be highly suitable for thermal management for such application, due to their superior thermo-dynamic properties and a relatively high surface area density, along with high permeability to cooling fluids. The heat transfer performance of such porous metals depends on their structural characteristics, which are dictated by the manufacturing processes. Although there has been research and development across this field, work continues as new techniques for making this type of heat sink are still being developed. Zhao et al. (2005) developed the Lost Carbonate Sintering (LCS) process for production of stochastic porous metals, porous copper being a leading example. The LCS process is a low cost method enabling direct control over porosity and pore size by combining powder metallurgy with the use of a leachable carbonate space-holder for pore development [1]–[9]. The base metal, copper, is mixed homogeneously with the space holder using classical mixing procedures; this is usually made complicated by the density difference between two primary materials; base metal and carbonate space holder [10]. After shaping (e.g. by pressing in a die), the component is then taken through the densification process by either hot pressing [1], [2], [10]–[12] or pressureless sintering. Finally, the space holder is eliminated from the sintered component using either a dissolution or decomposition technique. Zhang et al. (2008) discussed this phenomenon at length and finally concluded that either the dissolution or decomposition route may be an appropriate choice for carbonate removal after sintering, depending on the product dimensions and carbonate particle size. The selection also depends on whether production time or shrinkage is the main concern [1], [5].

A separate powder process, tape casting (TC), is normally industrially employed for application such as fabricating ceramic powders into single or multi layered (capacitors) sheets [1], [5]. It has been recently adapted to produce non-ceramic powders, both metals and polymers. It is often the preferred choice in developing and producing these products because of its suitability, scalability, relative simplicity, and low implementation cost compared to other alternative methods such as hot or dry pressing, injection moulding, and 3D printing / Additive manufacturing. However, tape casting of metallic powders is still in its early stages [10], [11], [13]–[16]. It is important to note that tape casting is highly dependent on the quality of the slurry (the powder suspended in a liquid) prior to casting. Tape casting of different materials requires different formulations of slurry; solvents, binders, plasticizers and dispersants to fabricate high quality sheets.

In the previous work [17] we reported a novel process which combines TC and LCS to fabricate thin sheets of double–layered copper; a thin layer of porous Cu laminated onto a dense copper sheet. Tape casting of a blend of copper powders and polymeric binders allowed the use of LCS with K_2CO_3

introduced as a space holder to control porosity and pore size. The method allows the flexibility to control the thickness of the layer, the porosity, pore size and shape of the tapes, yet thus far the influence of process parameters on the structure of the tapes has not been fully understood. This paper focuses on the structural characterisation of this type of porous tape, and seeks to study the effectiveness of the LCS and TC in tailoring the structure of the final component, introducing different processing routes and varying processing parameters such as the proportion of K_2CO_3 and the thickness of the tapes.

2. Material and Method

2.1 Raw Materials

Dendritic copper, Cu powder supplied by *Goodfellow, Cambridge, UK* and potassium carbonate, K_2CO_3 supplied by *Alfa Aesar, Lancashire, UK* were used as base metal and leachable space holder respectively. Figure 1 shows the morphology of these two primary powders. The powders were mixed in to a viscous slurry using the following chemicals; poly (methyl methacrylate) (PMMA) purchased from Alfa Aesar was used as binder, dibutyl Phthalate supplied by *Sigma Aldrich Company Ltd, Gillingha, UK* was used as a plasticizer. Azeotropic mixture of ethanol and 2-butanone at a ratio of 40:60 was used as a solvent during slurry preparation.
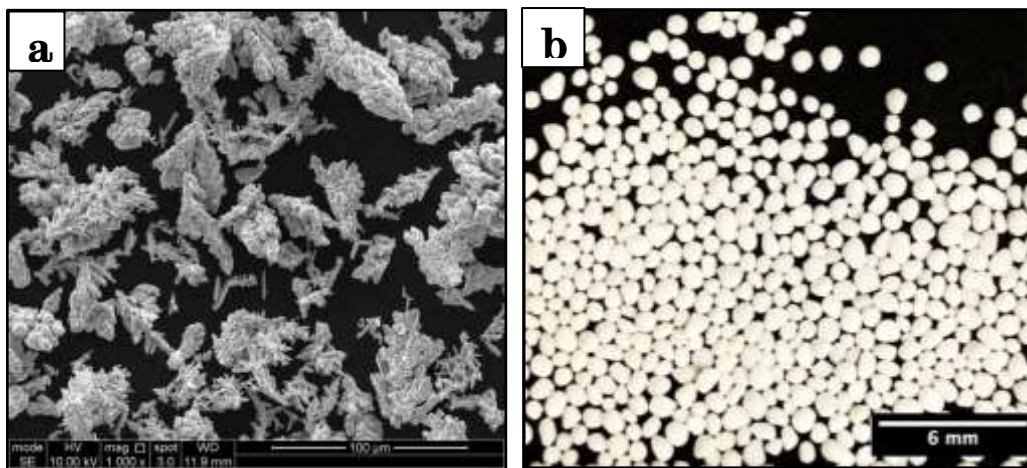

Figure 1: Morphology of two primary powders used to produce porous copper samples; a) dendritic Cu powder with average particle size of 50µm and b) K_2CO_3 space holder with particle sizes ranging from 110 - 738µm

2.2 Fabrication Procedure

The primary powders with addition of 0-50 wt% K_2CO_3 were mixed with polymeric binders of known quantities. To promote the formation of a homogenous slurry, the powders and polymeric binders were mixed using a high-energy speed mixer (Speedmixer™ Hauschild Flak Tek DAC 400FVZ) for 45 minutes at a speed of 1800 rpm.

Tape Casting and Drying; Once the right mixture was obtained, with suitable viscosity, the slurry was immediately tape cast while still homogenous and viscous. The thickness and width (fixed) were controlled by an adjustable doctor blade. The speed of the moving substrate was controlled by the motor. Two processing routes were developed to produce two batches of porous samples which are structurally different. A summarised flowchart in Figure 2 shows the two processing routes followed when tape casting the slurry, and a step-by-step procedure of each processing route (route A and B) is explained next.
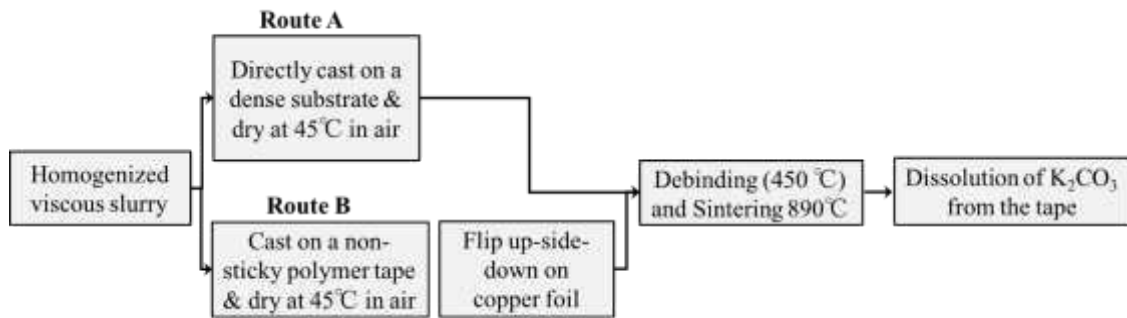

Figure 2: Two processing routes followed to produce porous copper samples by Lost Carbonate Sintering applied to Tape Casting

Processing route A: In this route, the slurry was cast directly onto a moving copper foil through an adjustable doctor blade on the tape casting machine. The thickness and the width of the slurry were controlled by the stationary doctor blade. The slurry was then allowed to partially dry in air for 3 hours while still on the tape caster set at 40 °C. The green tape was then debinded and sintered using a vacuum sintering furnace at 450 °C and 890 °C respectively following the heat treatment profile in Figure 5.

Figure 3: Schematic diagram of the tape casting process, a) a viscous slurry inside the hopper directly tape cast on to a moving dense copper substrate through an adjustable doctor blade, and b) double-layered green tape before debinding and sintering.

Processing route B: In this route, an additional step was added to the previous route (route A) during the tape casting process. This was done to obtain a different pore distribution as compared to route A. Here, the slurry was deposited on to a non-adhesive polymer film(silicone-mylar) instead of the

copper substrate and allowed to dry under air while still on the tape casting machine set at 40 °C. This tape allows the green copper layer to be easily peeled off after drying.
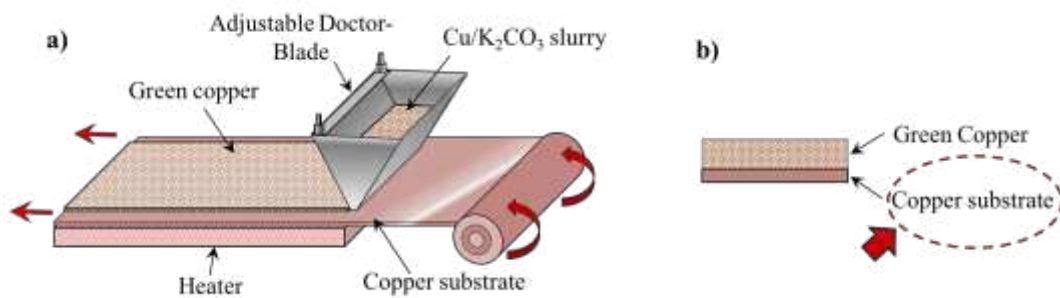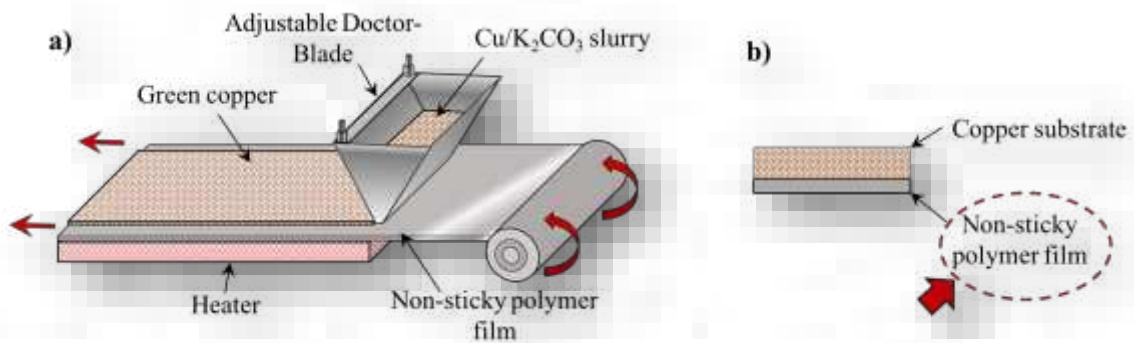

Figure 4: Schematic diagram of the tape casting process, a) a viscous slurry inside the hopper directly tape cast on to a moving dense copper substrate through an adjustable doctor blade, and b) double-layered green tape before debinding and sintering.

The solvent (azeotropic mixture of ethanol and 2-butanone) was lightly sprayed on the surface of the green tape to enhance bonding. The green tape was then immediately turned upside down (while still on the polymer film) on to the copper substrate and rolled down using a rubber roller to promote the formation of a good bond between the green section and copper foil. Similarly, the green samples were then taken through a debinding and sintering process following the heat treatment profile in Figure 5.
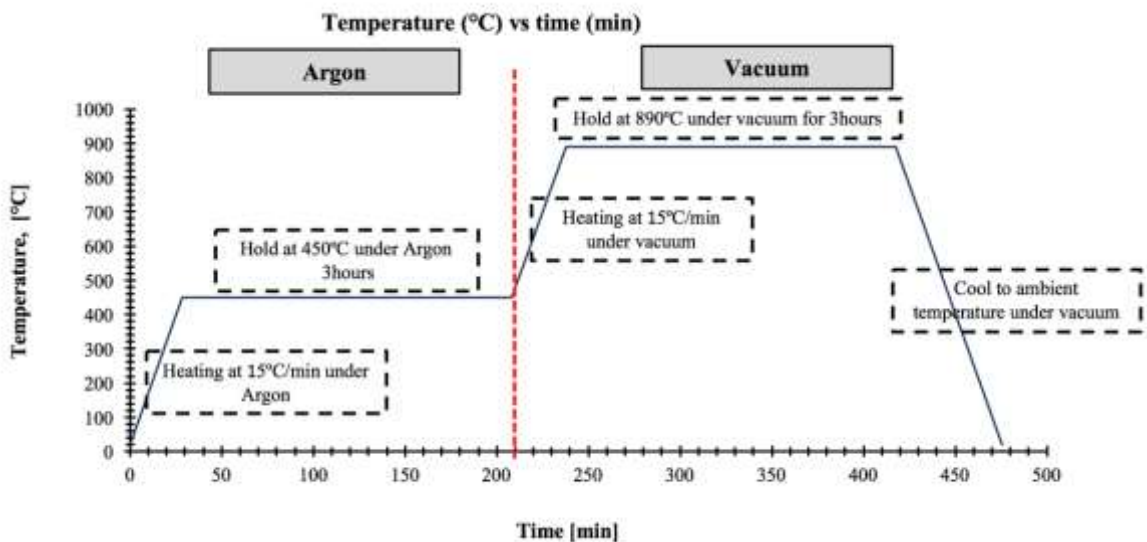

Figure 5: The heat treatment profile for debinding and sintering green copper tape.

To generate pores in the sheets and obtain a wide range of porosities, 10-50 wt% K_2CO_3 was added during processing across both routes. Table 1 shows the quantities of K_2CO_3 in terms of weight

percent, added to copper powder during production of samples with varying porosities. The pore size of K_2CO_3 particles ranged from 110 - 738µm.

Table 1: Amount of carbonate space holder added across the porous Cu samples produced

Processing Route	Amount of Carbonate Space-holder Added, (Wt.%)					
	Set 1 (0CuP)	Set 2 (10CuP)	Set 3 (20CuP)	Set 4 (30CuP)	Set 5 (40CuP)	Set 6 (50CuP)
A	0	10	20	30	40	50
B	0	10	20	30	40	50

NB: The sample nomenclature used is as follows; the first number is the weight percent K_2CO_3 added, the middle letters (CuP) refer to the fact that these are "porous copper", and the last letter (A or B) is the processing route employed.

The green tapes from both processing routes were debinded and sintered for 6 hours at 450 °C and 890°C respectively. To minimise oxidation, the tapes were debinded and sintered under argon and vacuum controlled environments at Wallwork Heat treatment LTD, Bury, UK using a controlled atmosphere sintering furnace. After sintering, the samples were allowed to cool to room temperature while still under vacuum. Finally, the carbonate space holder was removed from the sintered tapes by dissolution using warm water by stirring, and the final porous sample was dried under a dry hot air.

2.3 Characterisation of the Structure
2.3.1 Density Measurements

It is important to note that the density (ρ_a) of the samples analysed here was the bulk (apparent) density not the true (skeletal) density (ρ_m) of the metal making it up. To calculate the bulk density (ρ_a), the sample was first measured using Vernier callipers to obtain the total volume, V_a, (pore plus metal matrix). It was then weighed using an electronic weighing balance with a tolerance of 0.0001 g to obtain the true mass (m_m) of the porous sample (solid matrix). True volume (V_m) was also measured using a gas helium pycnometer *(Accupyc II 1340, Micromeritics)* to obtain the true density of the metal making up the structure, as this can help to assess it there is closed porosity which would be inaccessible to a cooling gas flow.

$$Vf_m = (1 - \frac{\varepsilon}{100}) \tag{1}$$

$$\rho_a = Vf_m\rho_m \qquad\qquad (2)$$

where Vf_m is the volume fraction of the copper matrix and ε is the volumetric or bulk porosity.

2.3.2 Porosity measurements

Two different techniques were implemented here to examine surface porosity and volumetric porosity of the porous sheets.

2.3.2.1 Surface porosity (2D)

Actual size image analysis was employed to analyse the structure of the porous sample mainly to study three different pore parameters; the total surface porosity, pore size distribution and pore shape. The samples were photographed in low to medium light conditions. The aim was to obtain images with a clear contrast between the pores and the continuous surface regions, both micropores and macropores. High resolution SEM micrographs were also used to evaluate the micropores. Images were calibrated and processed using ImageJ [18], [19]. An individual threshold was applied to each image, taking care not to alter the apparent pore diameter. Surface defects that appeared dark but were not identified as pores were manually removed. Particle analysis was also performed in ImageJ, obtaining the cross-sectional area, major and minor axes for each pore. Figure 6 shows the processed image where each pore was counted and measured as the closest-fitting ellipsis. The measurements obtained were analysed using Prism version 7 for Mac OS X 10.9, GraphPad Software, La Jolla California USA, which provided frequency analyses for each sample as well as K_2CO_3 particles.

$$P_{Total} = P_{Macro} + P_{Micro} \qquad\qquad (3)$$

Total surface porosity (P_{Total}) was calculated as the sum of micro porosity (P_{Micro}) and macro porosity (P_{Macro}). During processing the microporosity resulted from incomplete densification of the copper particles while the macroporosity is as a result of the leaching of the potassium carbonate. Both macroporosity and microporosity were analysed separately using *ImageJ* on images acquired by SEM.
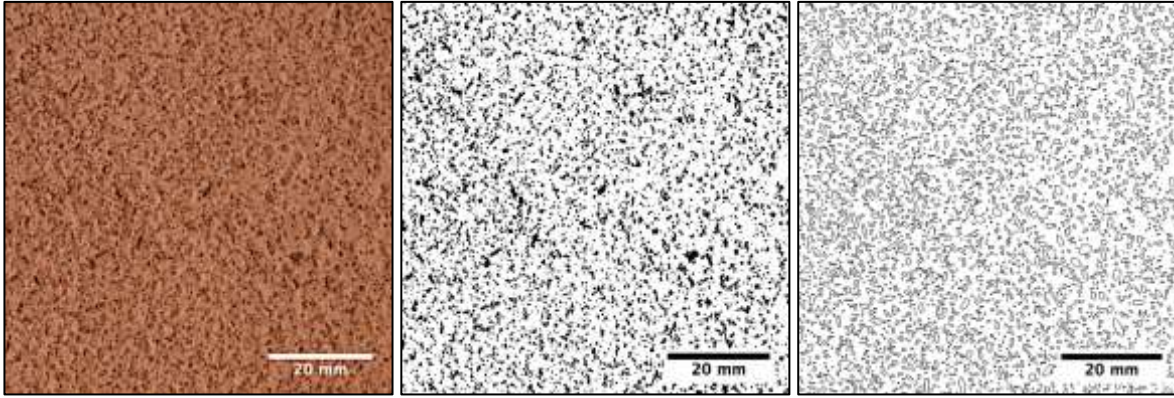
Figure 6: Actual size images obtained by Nikon D5300, and b) image processed by ImageJ and c) analysed by Prism version 7.

SEM images for macroporosity analysis were acquired at a lower magnification to have a wider distribution and a reasonably good number of the pores. For microporosity analysis, higher magnification images were captured. Each image was calibrated before analysis to ensure consistency throughout the images.

Pore size: Macro pore size of the samples is highly dependent on the particle size of the space holder (potassium carbonate). From the particle size measurements, the size of the particles ranges from 360 – 890 µm.

Average pore size and porosity can be obtained from these simple measurements shown in Figure 8. The average measurements of these parameters will always be less than it is on the sample.

2.3.2.2 Volumetric Porosity (3D)

A helium pycnometer (Accupyc 1340, Micromeritics) was employed to obtain the true porosity of the copper making up the porous copper samples (n=3) using the following equation:

$$\varepsilon = \left(1 - \frac{V_t}{V_a}\right) \times 100 \tag{4}$$

where ε is the volumetric or bulk porosity, V_t is the true volume of the porous samples measured using a helium pycnometer, V_a is the total volume of the porous sample (including the pores) measured using Vernier callipers with a resolution of 0.01 mm to measure the dimensions.

2.3.3 Micro X-ray Computed Tomography (CT) Scanning and Analysis

Three porous samples produced following processing route A; 20CuPA, 40CuPA and 50CuPA were selected for this investigation, as well as three samples produced following route B; 10CuPB, 30CuPB

and 50CuPB. All samples were scanned by a micro-CT scanner (*In vivo* scanner (Skyscan, 1076, *in vivo* micro-CT scanner, Skyscan NV Kontich Belgium). The porous copper was fixed on an expanded polystyrene foam having the specimen axis in common with the rotation axis of the system. Several trial scans were necessary in order to visualise all components of the porous sample by obtaining suitable settings for the system. Scan system settings used were as follows; full rotation over 180°, source voltage 100kV, current 10 W, rotation step 0.5° aluminium filter thickness 0.5 mm, exposure time 0.59 seconds, 4 frame averaging, isotropic pixel size 17.4 µm. Skyscan *NRecon* software was employed to reconstruct the images by means of an Itered back – projection algorithm. The generated images were then processed and analysed with the use of *CTAn* software and the calculations were mainly performed in Microsoft Excel.

3. Results and Discussion

The copper slurry was successfully tape cast on to a thin and dense copper substrate to obtain a double-layer green copper tape. The tapes were then sintered followed by a dissolution process to remove K_2CO_3 from the copper matrix hence obtaining a double-layered structure of a porous copper layer on a dense copper substrate. The structural characteristics of the porous sheets investigated are therefore presented and discussed below.

3.1 Microstructure

Scanning electron microscopy (SEM) analysis was employed to study the pore structure of the tapes. Figure 7 shows the SEM micrographs of the sintered porous tapes depicting the pore structure within the copper matrix. All SEM micrographs in Figure 7 were obtained by observing the sample from the top surface of the porous section, as it is directly after the sintering process, with no additional surface preparation. The copper particles appear to have adhered very well to each other forming a continuous structure of copper matrix (see Figure 7 (e) and (f)) after debinding and sintering at 450 °C and 890 °C under argon and vacuum respectively. It is clear from the images that addition of 10-50 wt% K_2CO_3 during processing generated macropores resembling the shape of K_2CO_3 particles. These macropores are interconnected to one another especially in samples with higher level of porosity, however, in sample with low porosities, macropores are mostly bridged by micropores produced as a secondary effect of incomplete densification of the sintered copper particles (Figure 7 (c)). Despite the fact that the pores resemble the shape of K_2CO_3 particles, the pore size revealed on the surface of the samples are less than is actually the case on the sample. In Figure 8 (a) and (b), the top surface on

the porous section was ground to reveal the actual pore size as well as internal pore morphology and pore wall morphology.

Here, pores with diameter $\geq 50\ \mu m$ are classified as macropores while pores $\leq 50\ \mu m$ as micropores. The micropores in the sheets have important effects: (1) during processing and (2) for the functionality of the component. During processing, when carrying out the debinding process on the green tapes, the decomposition gases escape the tape mainly through micropores. Such routes are also beneficial in the removal of K_2CO_3 from the metal matrix by dissolution. K_2CO_3 in solution escapes the samples through both the macropores and micropores. Sintering the component can results in copper particles bonded around the K_2CO_3 particles, therefore the K_2CO_3 particles are only accessible to water through micropores. During the use of the material, these micropores would also contribute to permeability of

the porous copper tapes to air by interconnecting with macropores hence bridging the cooling air between macropores.
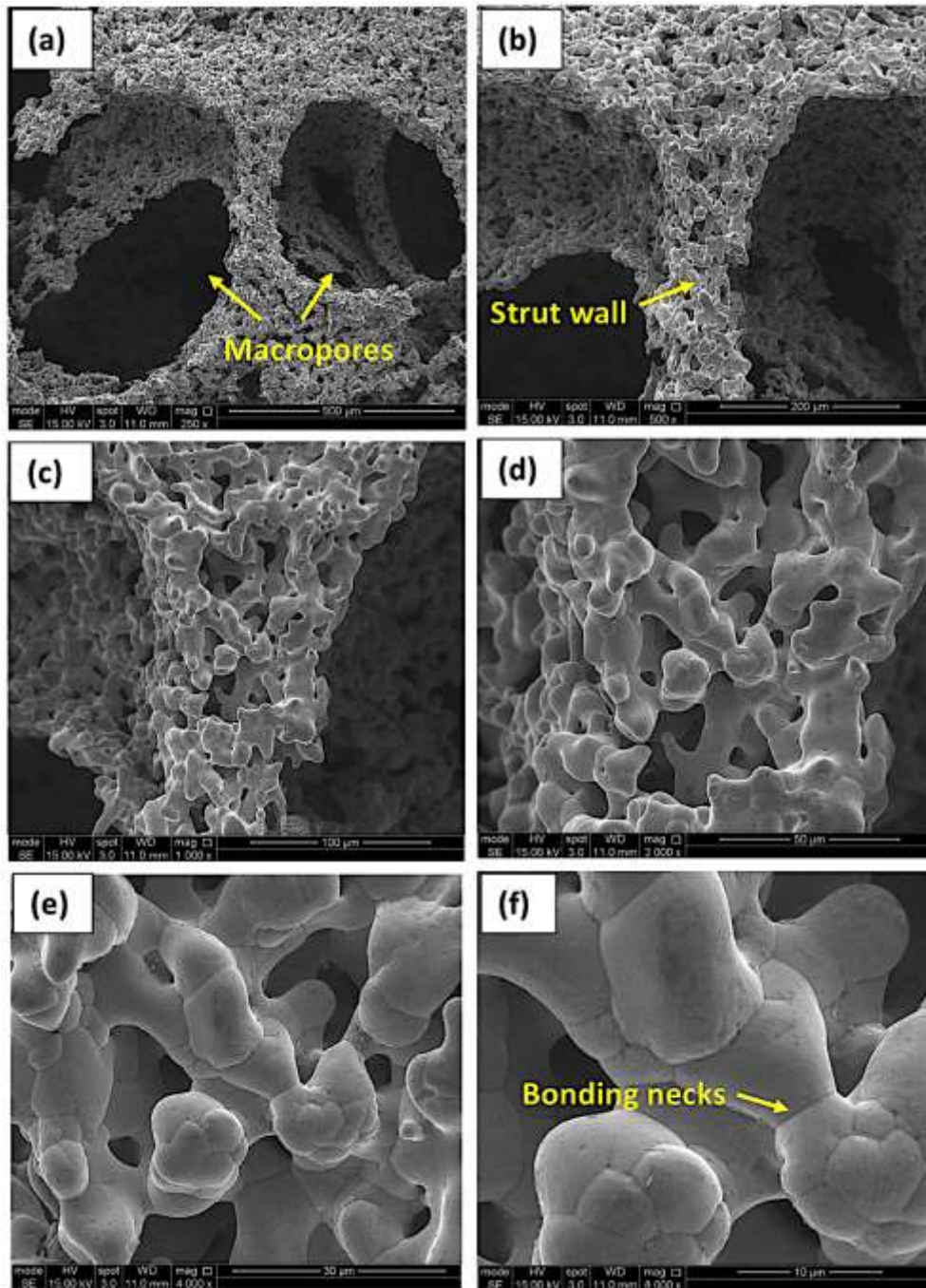

Figure 7: Top surface of porous copper samples showing the distribution of the macrpores from leachable carbonate space-holder, c) micropores resulting from incomplete densification and finally d) bonding necks of copper particles after sintering at 890 °C
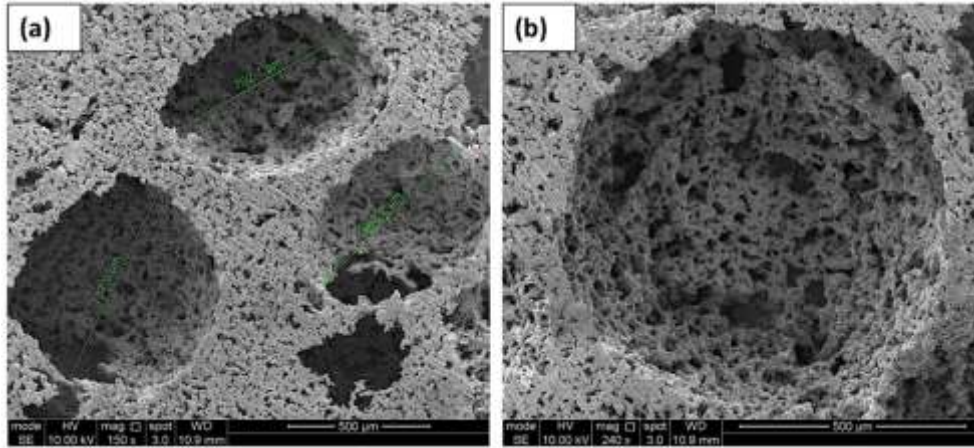
Figure 8: SEM micrographs of sintered tapes revealing the structure of the macropores; (a) and (b) ground sample to reveal the internal structure of the macropores generated by K_2CO_3

The shape of the dendritic copper used leads to the formation of irregular pore structures and rougher pore surfaces (see Figure 7 (a) and (c)). During the sintering process (at 890 °C), it was found out that ~5% of K_2CO_3 (melting point = 891°C) was removed from the component after 2 hours. As the K_2CO_3 is removed the support it provides is reduced, thus permitting a slight distortion on the final pores during sintering.

3.2 Density and volumetric porosity

Relative density is one of the most significant parameters for determining the mechanical and physical properties of a porous metal. In porous metals, porosity is directly related to density, whereas in homogenous or single-phase material the density is that of the bulk material. As part of this work, it was important to find the relative density of the porous samples produced here. The relative density was measured by employing volume fraction (V_m) and true densities of the bulk metal, where the helium pycnometer was used, taking the density of the solid material to be $\rho = 8.96\ g/cm^3$. The appropriate equations are given in the experimental section and the results of the relative density (and volumetric porosity) plotted against amount K_2CO_3 (in weight percent) and are presented in Figure 9.

Eleven samples produced by following processing route A (0CuP, 10CuPA, 20CuPA, 30CuPA, 40CuPA and 50CuPA) and B (0CuP, 10CuPB, 20CuPB, 30CuPB, 40CuPB and 50CuPB) were investigated. It is clear from the graph that the density of the porous tapes decreases with the addition of the K_2CO_3 space holder (wt.%). At the start, the porous tape produced without addition of K_2CO_3 (0CuP) achieved a density of 4.46 g/cm^3, which is the highest density obtained from the samples considered in this investigation. The density is clearly less than the bulk density of copper ($\rho_{Cu} = 8.96$ g/cm^3). In summary, 10CuPA (10 wt.% added) achieved a density of 3.31 g/cm^3 while 20CuPA, 30CuPA and 40CuPA achieved densities of 2.69 g/cm^3, 2.23 g/cm^3 and 1.94 g/cm^3 respectively.

10CuPB achieved a density of 3.00 g/cm^3, while 20CuPB, 30CuPB and 40CuPB achieved a density of 2.36 g/cm^3, 1.88 g/cm^3 and 1.75 g/cm^3. In addition, 50CuPB with a higher percentage of porosity achieved the lowest density of 1.65 g/cm^3, while 50CuPA achieved 1.75 g/cm^3. Generally, the samples produced by route B achieved lower densities compared to samples produced by route A. Their densities decreased from 3.00 g/cm^3 to 1.65 g/cm^3 by addition of 10-50 wt.% K$_2$CO$_3$, while the density of samples processed by route A decreased from 3.28 g/cm^3 to 1.75 g/cm^3. The lower densities of samples produced by processing route B might have resulted from incomplete bonding, which was observed between the porous layer and the dense substrate. This incomplete bonding of the two layers resulted from the approach used which involved first tape casting the 'porous layer' then bonding this to the dense substrate at a later stage (see section 2.2). The porous layer displayed an uneven surface caused by K$_2$CO$_3$ space holder protruding from the surface. During sintering this side did not adhere well to the dense substrate which left some macropores contributing to porosity within the boundary area. This also contributed to lower levels of density in the samples produced by route B. However, the layers (porous and dense layer) of the samples produced by route A adhered well, leaving a high amount of micropores compared to macropores within the boundary layer, and, relatively, increasing the densities of samples produced by route A.
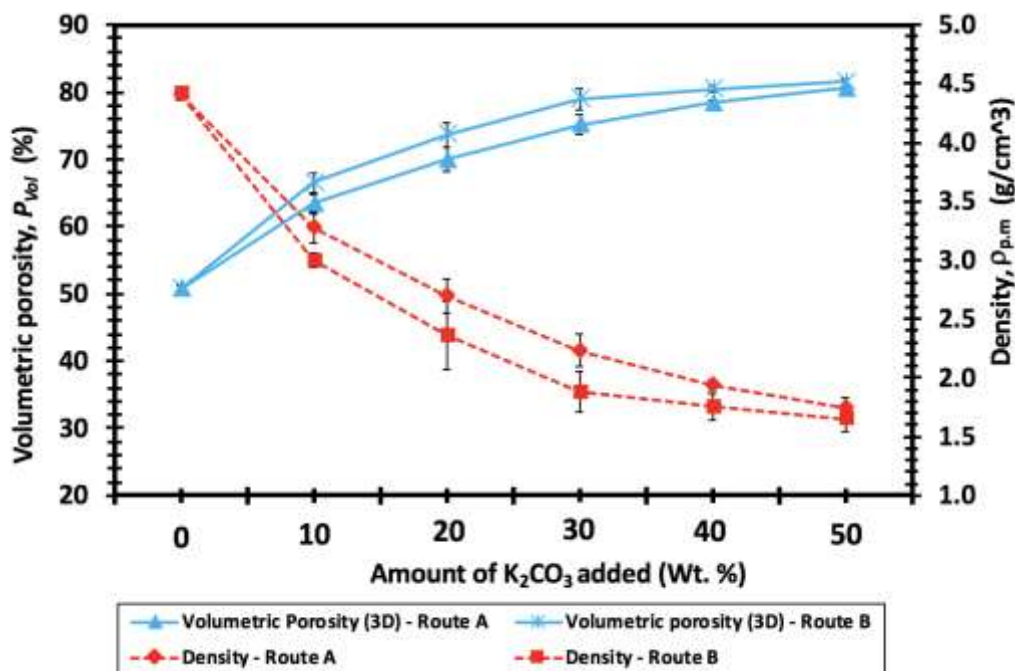

Figure 9: Density of porous copper tapes produced by both processing route A and B

There is a direct relationship between porosity and density of the materials tested as clearly seen in Figure 9. The density variations in the samples investigated here (between the bulk copper powder and samples with different amounts of space holder added) are due to (i) incomplete densification of the copper powder, (ii) macroporosity generated by K$_2$CO$_3$ and (iii) the presence of some defects resulting from processing. Incomplete densification, as a means to generate porous materials, is

usually controlled by changing the processing parameters such as sintering temperature, sintering time, compaction pressure, and material parameters such particle size, particle shape etc. In this study, the effect of incomplete densification was not directly explored, but it was present as a secondary effect, and was also a necessary requirement to obtain a structure with interconnected pores. The processing and materials parameters were kept constant throughout fabrication of the samples, and therefore, the porosity due to incomplete sintering was only affected by the introduction of K_2CO_3 space holder. This type of porosity was found to be high in samples where a larger amount of K_2CO_3 space holder was added. Randomly distributed defects appearing on the surface might be due to processing (for example, bubbles present from the mixing stage). It is possible that some binder components, especially PMMA and triphenyl phosphate, were left undissolved, and trapped within the matrix during processing (i.e. debinding and sintering). Later, decomposition of these lumps might have left behind some fine defects as additional pores. Rearrangement of the Cu matrix resulting in surface tearing as the binders are burnt out of the sample will also leave gaps which are partially occupied by the copper.

Some air pockets were observed within the green section and also between the green layer and the dense substrate. During debinding and sintering the air pockets close to the sample surface burst on the surface leaving some defects.

3.3 Surface porosity

The measured microporosity and macroporosity for each sample are presented in Figure 11, where Figure 11 (a), and (b), represent the total microporosity and macroporosity of the samples from both processing routes respectively. The total surface porosity was calculated by the sum of micro and macroporosity, and is presented in Figure 10. Even though individually the microporosity decreased and macroporosity increased with addition of K_2CO_3, the total surface porosity increased with addition of K_2CO_3 during processing. Generally, samples produced by processing route B achieved a higher percentage of surface porosity compared to the samples produced by route A, with the difference increasing as higher amounts of K_2CO_3 are added.
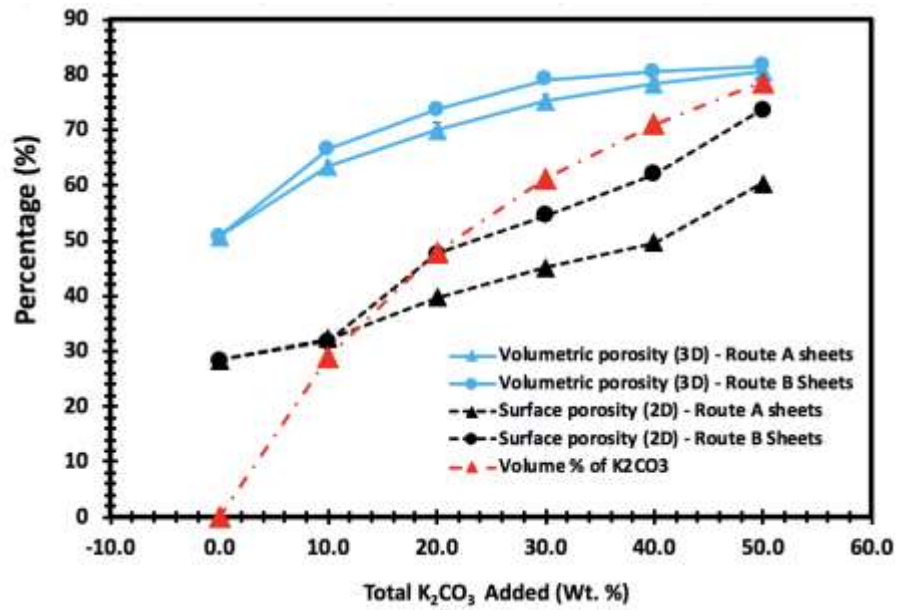
Figure 10: The two graphs showing the effect of K_2CO_3 addition on the surface porosity and volumetric porosity (3D) porosity of porous samples produced by both processing route A and B.
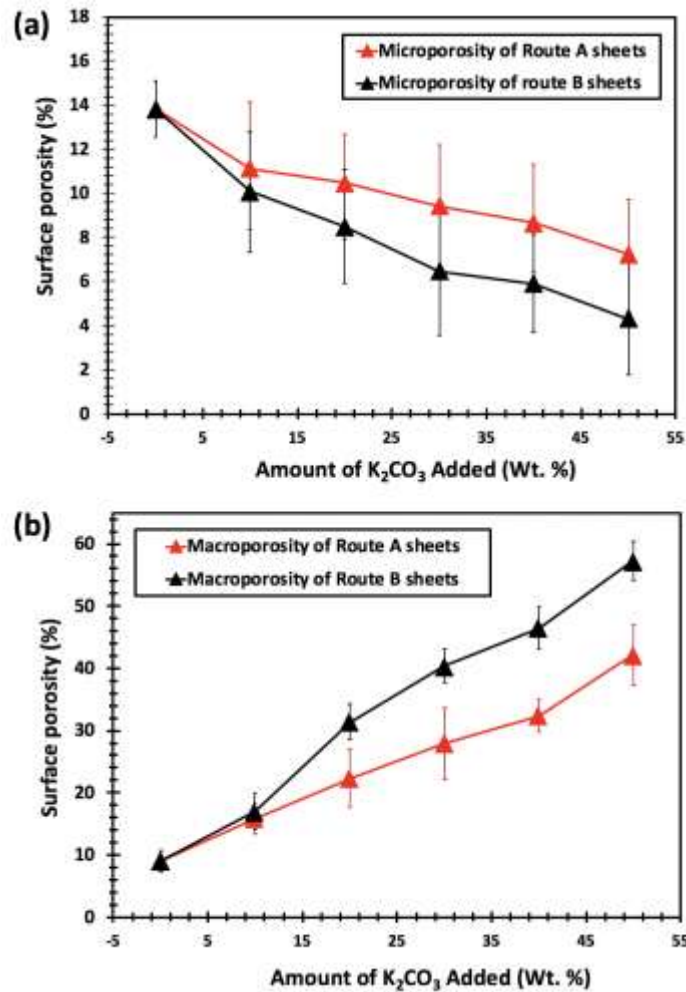
Figure 11: Surface porosity of porous copper tapes produced by both processing route A and B: (a) microporosity and (b) macroporosity.

Addition of 10 wt.% K_2CO_3 generated the same amount of total surface porosity on 10CuPA and 10CuPB. The total surface porosity increased with the addition of 20-50wt.% K_2CO_3 across the samples produced by both routes A and B. However, samples produced by route B achieved higher percentage of total surface porosity compared to the samples produced by route A for a similar amount of K_2CO_3 added. The difference in the total surface porosity among the samples from both routes was clear with the addition of 20-50wt.% K_2CO_3, of which 20 wt.% K_2CO_3 and 30 wt.% K_2CO_3 generated a total surface porosity of 32.8% and 37.3% on samples produced by route A compared to 38.9% and 46.8% of route B samples respectively. By adding 40 wt.% and 50 wt.%, a porosity of 41.1% and 49.3% was generated on route A samples compared to 52.4 and 61.6% on route B samples respectively. After addition of 50 wt.% K_2CO_3 route B samples were 12.3% more porous compared to route A samples. At this stage, the samples produced by route B were generally more porous on the top surface compared to the samples produced by route A.
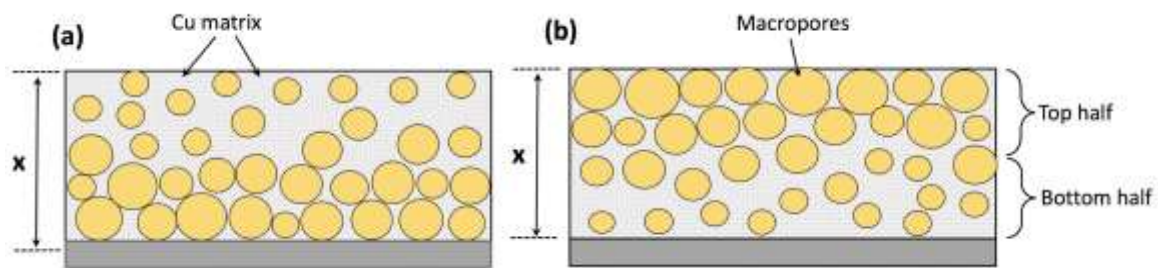
Figure 12: A Schematic diagram showing the pore size distribution across the thickness of tapes produced by processing routes (a) A and (b) B.

A schematic diagram in Figure 12 represents how the macropores are distributed across the samples produced by the two processing routes, Figure 12 (a) route A and (b) route B. It was found that macropores generated by K_2CO_3 are concentrated in the bottom-half of the sample rather than the top-half for all the samples produced by route A and vice-versa for samples produced by route B. This scenario is further discussed in section 3.5 and 3.6.

3.4 Volumetric Porosity

Figure 10 shows both the total surface porosity and volumetric porosity plotted against the amount of K_2CO_3 added to the sample during processing in weight percent (wt.%). Like surface porosity, volumetric porosity increased with the addition of the K_2CO_3. 0CuP achieved the lowest volumetric porosity of 50.7 %, while 10CuPA and 10CuPB achieved slightly higher porosity of 63.4 % and 66.5% respectively. 30CuPA and 30CuPB attained 75.2% and 79.0%. The highest percentages of volumetric porosity were achieved by 50CuPA and 50CuPB which recorded 80.5% and 81.5% respectively.

It was observed from the graph that, by adding small amounts of K_2CO_3, volumetric porosity increased gradually by larger variations in both sets of samples, either produced following route A or route B. However, adding large amounts of K_2CO_3 caused a relatively small further variation of volumetric porosity. The reason for this could be due to the distortion of the macropores, which was noticeable in the porous sample after sintering, especially in the samples with a higher percentage of porosity. In this case, addition of larger amounts of K_2CO_3 causes higher amounts of shrinkage as the smaller amount of matrix is lest mechanically stable and able to retain the structure. Figure 13 depicts the SEM micrograph of distorted macropores resulting when larger amounts of K_2CO_3 (X wt.% $K_2CO_3 \geq 50$ wt.% K_2CO_3) was added during processing.

The SEM micrograph in Figure 13 reveals the structure of the sintered tapes indicating that during sintering the shape of the macropores in the final component is distorted. Figure 13 (b) shows partially

removed K_2CO_3 after sintering at 891°C under vacuum. The reason for the shape of the curves (blue lines) in Figure 10 could be that, after addition of smaller amounts of K_2CO_3 most of the sample densified (mostly Cu particles) during sintering, hence providing mechanical strength which resists distortion in shape and retains macropores generated by the starting shape of the K_2CO_3. However, addition of large amounts of K_2CO_3 space holder means lower Cu and less remaining material to provide strength.
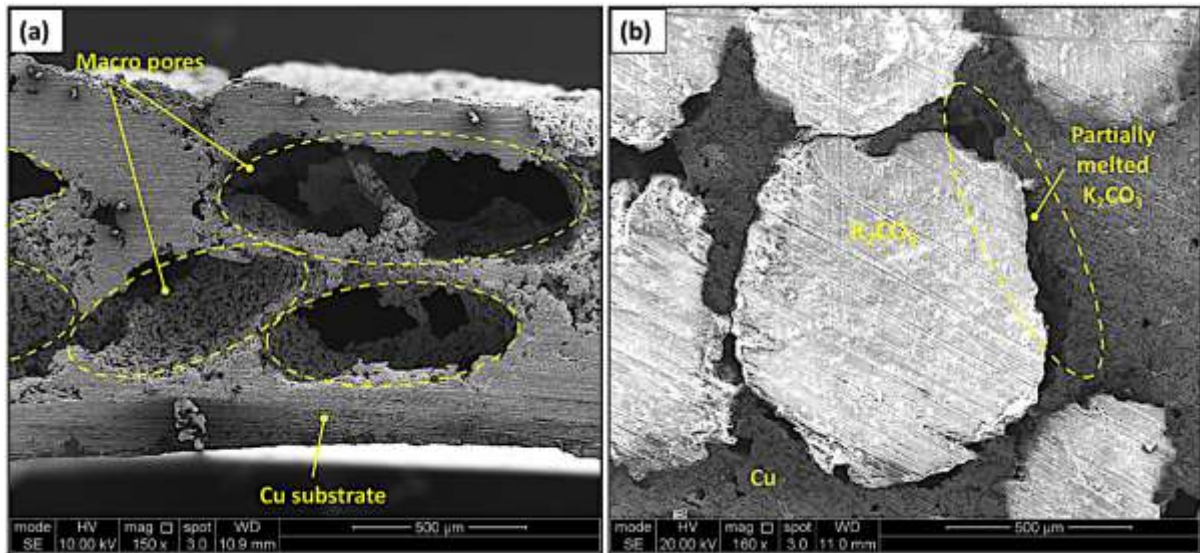

Figure 13: SEM micrograph revealing the structure of the pores across the thickness of the sample. The pores are oval-shaped, which resulted from shrinkage in the through thickness direction.

The constraint of the already dense Cu sheet, which provides support against reduction in lateral dimensions may be another reason why densification of the sample occurs mainly in the through thickness direction (from the top surface of the sheet to the Cu substrate or the base of the sample) resulting in a decrease in the rate at which volumetric porosity increases when larger amounts of space holder is added, hence the shape of the curve.

Addition of space holder greater than 50 wt.% K_2CO_3 resulted in the formation of a fragile porous structure which made it very difficult to cut or machine for further characterisation. This was due to weaker struts making the whole sample fragile especially after dissolution of the space holder. It was then decided that addition of K_2CO_3 space holder should be constrained to $\leq$ 50 wt.% K_2CO_3 to compromise between the volumetric porosity and the handling strength.

It is evident from the SEM micrograph in Figure 13 that, only a small percentage ($\approx$ 5 %) of K_2CO_3 is removed during sintering at a temperature ($T_{melting}$ = 890 °C) very close to the melting temperature of K_2CO_3 ($T_{melting}$ = 891°C). This shows that the space holder is not only removed by dissolution but

also by a thermal mechanism which may be evaporation or melting. The TGA results also indicate that K_2CO_3 started to be removed during sintering, allowing the metal matrix to densify mainly along the through thickness direction forming oval shaped pores. This results in a reduction of the pore volume during sintering therefore affecting volumetric porosity more than surface porosity. As shown in Figure 10, volumetric porosity increases more with weight% of K_2CO_3 at the start, but then increases at a slow rate with an increase in weight% of K_2CO_3 added.

3.5 Pore distribution by Image Analysis - 2D

At the beginning of this study, the samples were only produced by processing route A, where the slurry was directly fabricated on the copper substrate through the doctor blade as shown in Figure 3, then sintered. SEM micrograph analysis was employed to carry out initial assessment of the pore distribution across the thickness of each sample. The samples were sectioned and imaged by SEM hence allowing porosity measurement using image analysis. By dividing the thickness of each sample in the image into two halves; bottom and top half porosity was measured in sections, and the results are presented in Table 2. It was found that macropores generated by K_2CO_3 are concentrated in the bottom-half of the sample rather than the top-half for all the samples produced by route A. 20CuPA achieved 38.6 ± 2.3 % of the macropores concentrated in the top-half compared to 61.4 ± 2.6 % of the macropores mainly in the bottom-half, while 40CuPA achieved 35.6 ± 2.1% of the macropores mainly in the top part compared to 64.4 ± 2.6 % in the bottom-half. 50CuPA also obtained a similar pore distribution where 39.2 ± 2.5 % of the macropores were concentrated in the top-half compared to 60.8 ± 2.9 % in the bottom-half. This is likely to be due to the settling out of the particles during the tape casting process and while the binder is still fluid to some extent afterwards.

Table 2: Average pore distribution across the thickness of the porous samples produced following processing route A and B.

Manufacturing routes	Samples	Top half porosity (%)	Bottom half porosity (%)
Processing Route A	20CuPA	38.6 ± 2.3	61.4 ± 2.6
	40CuPA	35.6 ± 2.1	64.4 ± 2.7
	50CuPA	39.2 ± 2.5	60.8 ± 2.9
Processing Route B	20CuPB	58.3 ± 2.8	41.7 ± 3.1
	40CuPB	61.7 ± 2.5	38.3 ± 3.2
	50CuPB	60.2 ± 2.6	39.8 ± 3.3

Ideally, considering the design of a heat sink, samples with higher porosity in the top-half of the component than in the bottom-half would be expected to have better heat transfer performance. The higher density of metal near the solid would increase the local thermal conductivity, facilitating transport of heat away from this region, while the greater and more open porosity facing the cooling fluid would allow it to flow more easily and provide easier access to the surface for heat transfer. By introducing processing Route B shown in Figure 4, the pore distribution was inverted, resulting in a more porous top-half than the bottom-half as clearly revealed in the Table 2. 20CuPB showed a higher percentage of macropores in the top-half of 58.3 ± 2.8 % compared to 41.7 ± 3.1 % in the bottom-half. 40CuPA also achieved a similar pore distribution where 61.7 ± 2.5 % of the macropores were concentrated in the top-half and 38.3 ± 3.2 % in the bottom-half. Also, 50CuPB obtained 60.2 ± 2.6 % of the macropores concentrated at the top-half and 39.8 ± 3.3% in the bottom-half. Both route A and B samples were taken through further investigation, most importantly heat transfer analysis. The total surface porosity of samples processed by route B is clearly higher than that of samples produced by processing route A as observed from Figure 10.

3.6 Pore distribution by microCT analysis – 3D

It was also necessary to study the pore distribution across the samples in a 3D form, hence microCT analysis was employed. From the analysis, the plots of pore volume versus thickness were generated representing how the pores (especially the macropores) are distributed in a 3D form as shown in Figure 14. Six samples were systematically selected for this investigation; 20CuPA, 20CuPB, 40CuPA, 40CuPB, 50CuPA and 50CuPB.
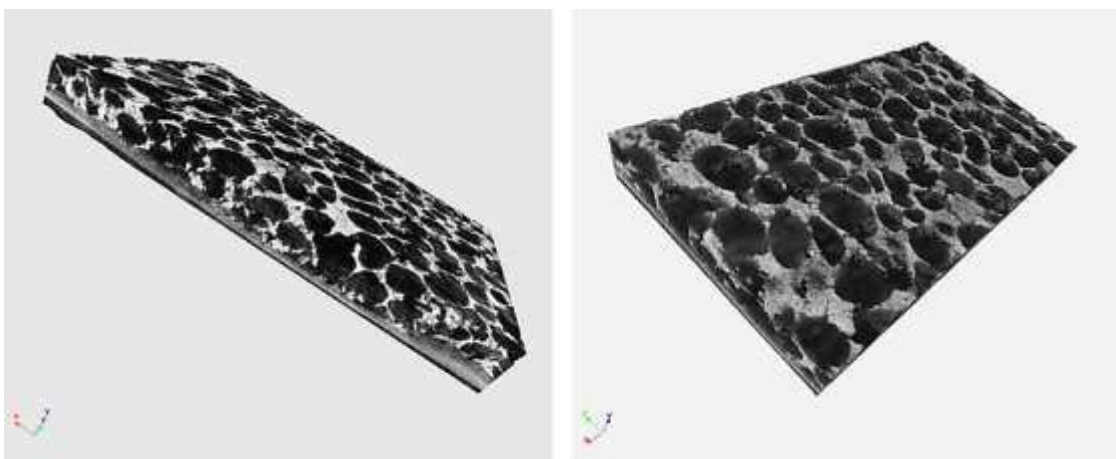

Figure 14: 3D images of porous copper sheets revealing the pore distribution across the thickness of 40CuPA.

As depicted in Figure 15, the results agree with the image analysis (2D) results discussed earlier in section 3.5, where the samples produced by processing route A have a higher percentage of macropores in the bottom-half of the sintered samples than in the top-half while the samples from

processing route B recorded a lower percentage of the macropores in the bottom-half of the sample compared to the top-half. Figure 15 (a), (c) and (e) represent 20CuPA, 40CuPA and 50CuPA and Figure 15 (b), (d) and (f) represent samples 20CuPB, 40CuPB and 50CuPB respectively. Given that pores with a volume greater than 205, 670 μm^3 are classified as macropores in this work, the rectangles with a dotted red outline are used in these plots to highlight the regions of macropores within the plots, either within the bottom-half or the top-half of the tested samples as labelled.
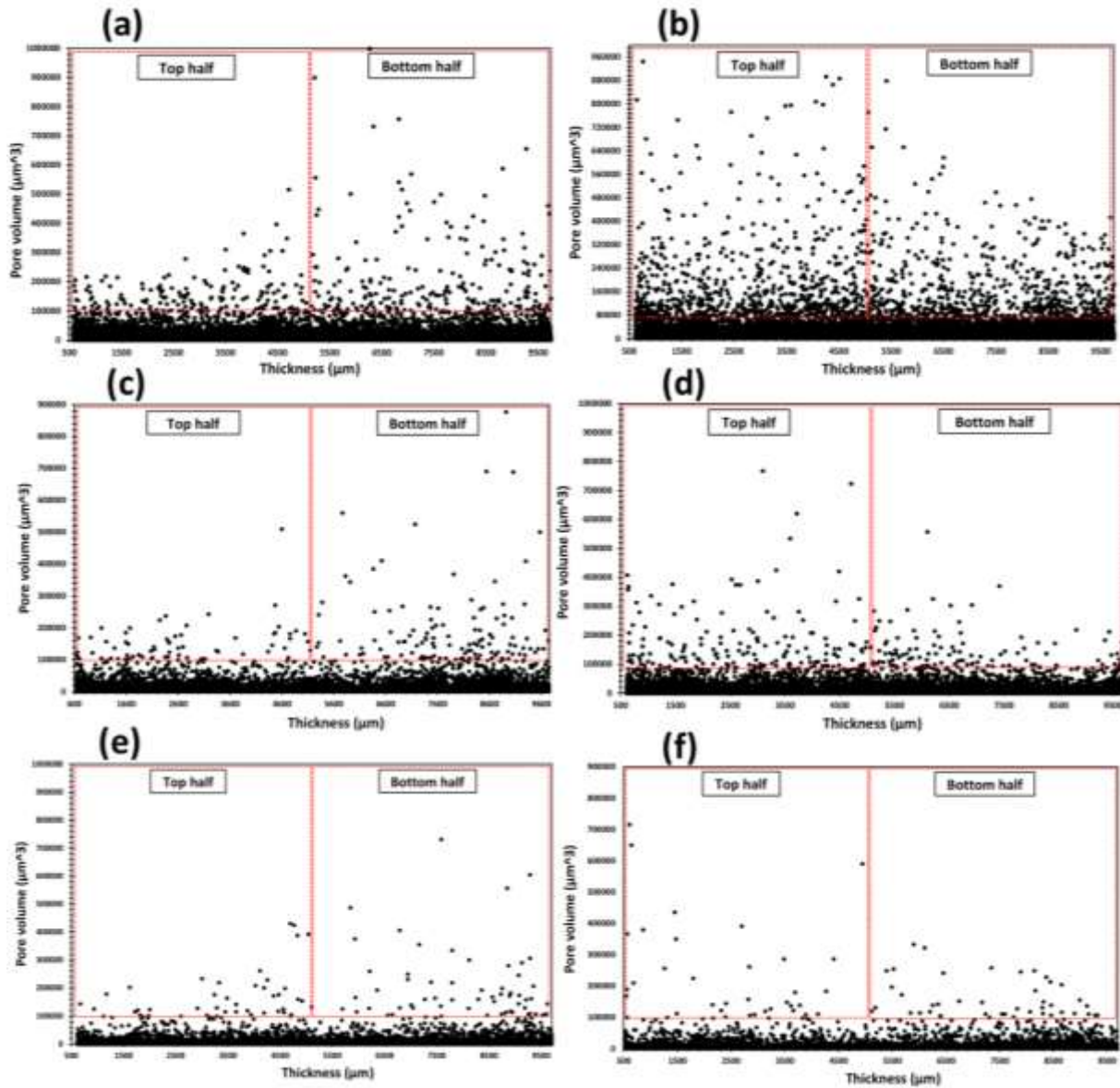

Figure 15: Pore volume distributions of the micropores and macropores across the thickness of the porous tapes (a) 20CuPA, (b) 20CuPB, (c) 40CuPA, (d) 40CuPB, (e) 50CuPA and (f) 50CuPB.

The pore distribution was mainly influenced by two processing factors. Even though the 99.9% pure Cu (density = 8.96 g/cm^3) used in this study is denser than the K_2CO_3 (density = 2.43 g/cm^3), the mixture of the organic binders ((ρ_{PMMA} = 1.18 g/cm^3, ρ_{Ethnol} = 0.79 g/cm^3, $\rho_{2\text{-Butanol}}$ = 0.81 g/cm^3, ρ_{DBP} = 1.05 g/cm^3 and ρ_{TPP} = 1.21 g/cm^3 at 20 °C) is half as dense as the K_2CO_3 space holder. After casting

the slurry, the K_2CO_3 tends to sink towards the Cu substrate while the slurry is still viscous, resulting in higher concentration of K_2CO_3 in the bottom-half compared to the top-half, thus leading to an inhomogeneous distribution of the macropores in the final porous component.

4. Conclusion

Thin sheets of porous copper heatsink with a double-layered structure were successfully produced by LCS applied to tape casting. The double-layered structure consists of a thin porous layer of copper, integrated with a dense Cu substrate. Structural parameters of the porous Cu such as pore shape and distribution, surface porosity and volumetric porosity were controlled by addition of 0 - 50 wt.% leachable K_2CO_3 space holder during processing. Two processing routes were explored in this study: processing route A and B. Both processing routes were introduced to alter the structural properties of the porous Cu samples. For processing-route A, addition of 0 – 50 wt.% K_2CO_3 increased surface porosity from 28.3% to 60.3% and volumetric porosity from 50.7% to 80.5%. It also achieved a density decrease in the range of 4.46 to 1.75 g/cm^3. Porous sheets produced following processing route B achieved surface porosity and volumetric porosity ranging from 28.3% to 73.6% and 50.7% to 81.54% respectively. Both types of porosities increased with addition of carbonate space holder in the range of 0 – 50 wt.% K_2CO_3. The porous sheets achieved a density decrease of 4.46 g/cm^3 to 1.65 g/cm^3 and thickness that ranged between 0.74 mm and 1.61 mm. Due to an increased surface porosity of component produced by route B over route A, the component has the potential to perform better in transferring heat thus good for heat transfer application. The future work will concentrate on the investigation of the heat transfer performance of such double-layered tapes.

Data Availability

The raw/processed data required to reproduce these findings cannot be shared at this time as the data also forms part of an ongoing study.

References

[1] Y. Y. Zhao, T. Fung, L. P. Zhang, and F. L. Zhang, "Lost carbonate sintering process for manufacturing metal foams," *Scr. Mater.*, vol. 52, no. 4, pp. 295–298, 2005.

[2] A. M. Parvanian, M. Saadatfar, M. Panjepour, A. Kingston, and A. P. Sheppard, "The effects

of manufacturing parameters on geometrical and mechanical properties of copper foams produced by space holder technique," *Mater. Des.*, vol. 53, pp. 681–690, 2014.

[3] D. J. Thewsey and Y. Y. Zhao, "Thermal conductivity of porous copper manufactured by the lost carbonate sintering process," *Phys. Status Solidi Appl. Mater. Sci.*, vol. 205, no. 5, pp. 1126–1131, 2008.

[4] L. Zhang, D. Mullen, K. Lynn, and Y. Zhao, "Heat Transfer Performance of Porous Copper Fabricated by the Lost Carnonate Sintering Process," *Mater. Res. Soc. Symp. Proc.*, vol. 1188, 2009.

[5] L. P. Zhang and Y. Y. Zhao, "Fabrication of high melting-point porous metals by lost carbonate sintering process via decomposition route," *Proc. Inst. Mech. Eng. Part B J. Eng. Manuf.*, vol. 222, no. 2, pp. 267–271, 2008.

[6] Z. Xiao and Y. Zhao, "Heat transfer coefficient of porous copper with homogeneous and hybrid structures in active cooling," *J. Mater. Res.*, vol. 28, no. 17, pp. 2545–2553, 2013.

[7] P. M. Shahzeydi Hosein Mohammad, "Production and charactirization of hihly porous copper foams synthesized by sodium carbonate space holder," pp. 90–95, 2013.

[8] A. M. Parvanian and M. Panjepour, "Mechanical behavior improvement of open-pore copper foams synthesized through space holder technique," *Mater. Des.*, vol. 49, pp. 834–841, 2013.

[9] Z. Xiao, "Heat transfer , fluid transport and mechanical properties of porous copper manufactured by Lost Carbonate Sintering," University of Liverpool, 2013.

[10] T. Guillemet, J. F. Silvain, J. M. Heintz, N. Chandra, and Y. F. Lu, "Fabrication By Tape Casting and Hot Pressing of Copper Diamond Composite Films," *Composites*, pp. 1–5, 2011.

[11] P. M. Geffroy, T. Chartier, and J. F. Silvain, "Preparation by tape casting and hot pressing of copper carbon composites films," *J. Eur. Ceram. Soc.*, vol. 27, no. 1, pp. 291–299, 2007.

[12] T. Schubert *et al.*, "Interfacial design of Cu/SiC composites prepared by powder metallurgy for heat sink applications," *Compos. Part A Appl. Sci. Manuf.*, vol. 38, no. 12, pp. 2398–2403, 2007.

[13] M. Cans, H. Hamdam, Y. Öner, and J. Bidaux, "Tape Casting of Copper Alloys for Tribological Applications," *Euro PM2008 - Adv. Powder Metall.*, no. October, pp. 27–32, 2015.

[14] Y. Tang, S. Qiu, M. Li, and K. Zhao, "Fabrication of alumina/copper heat dissipation substrates by freeze tape casting and melt infiltration for high-power LED," *J. Alloys Compd.*, vol. 690, pp. 469–477, 2017.

[15] J. Ru, B. Kong, H. Zhu, Z. Shi, and D. Z. Tongxiang Fan, "Microstructure, capillary performance and gas permeability of biporous copper fabricated by tape casting," *Powder Technol.*, vol. 256, pp. 182–187, Apr. 2014.

[16] A. G. Straatman, N. C. Gallego, Q. Yu, and B. E. Thompson, "Characterization of Porous Carbon Foam as a Material for Compact Recuperators," no. 42401. pp. 367–373, 2006.

[17] M. Mosalagae, R. Goodall, and M. Elbadawi, "Tape casting and lost carbonate sintering processes for production of heat sinks for portable electronics," *Adv. Mater. Lett.*, vol. 8, no. 7, pp. 807–812, 2017.

[18] J. Schindelin *et al.*, "Fiji: an open-source platform for biological-image analysis," *Nat Meth*, vol. 9, no. 7. Nature Publishing Group, a division of Macmillan Publishers Limited. All Rights

Reserved., pp. 676–682, Jul-2012.

[19]   J. Schindelin, C. T. Rueden, M. C. Hiner, and K. W. Eliceiri, "The ImageJ ecosystem: An open platform for biomedical image analysis," *Mol. Reprod. Dev.*, vol. 82, no. 7–8, pp. 518–529, 2015.

[20]   R. Goodall, "Thermomechanical Properties of Highly Porous , Fire-Resistant Materials," 2003.